J Therm Anal Calorim (2012) 108:253–262
DOI 10.1007/s10973-011-1584-8

Structure characterization and spectroscopic investigation of ciprofloxacin drug

Nadia E. A. El-Gamel · M. F. Hawash · M. A. Fahmey

Received: 8 March 2011 / Accepted: 8 April 2011 / Published online: 26 May 2011

Abstract Ciprofloxacin (CPF, $C_{17}H_{18}FN_3O_3$) drug is used in the treatment of some bacterial infectious diseases. The drug was investigated using thermal analysis (TA) measurements (TG/DTG) and electron impact mass spectral (EI-MS) fragmentation at 70 eV techniques. Furthermore, the drug was characterized and investigated by other spectroscopic tools as IR, UV–Vis, ^{1}H-, and ^{13}C-NMR. Semi-empirical MO calculation using PM3 procedure has been carried out on neutral molecule and positively charged species. The calculations included, bond length, bond order, bond strain, partial charge distribution, ionization energy, and heat of formation (ΔH_f). The PM3 procedure provides a basis for fine distinction among sites of initial bond cleavage, which is crucial to the rationalization of subsequent fragmentation of the molecule. The mass spectra and thermal analysis fragmentation pathways were proposed and compared to each other to select the most suitable scheme representing the correct fragmentation of this drug. From EI-MS, the main primary cleavage site of the charged molecule is that due to C–COOH bond cleavage with H-rearrangement to skeleton and CO_2 loss which can further decompose by piperazine loss. Thermal analysis of the neutral form of the drug reveals the high response of the drug to the temperature variation with very fast rate. Thermal decomposition has carried out in several sequential steps in the temperature range 40–650 °C. The initial thermal decomposition is similar to that obtained by mass spectrometric fragmentation (C–COOH fragment) but differ in that a rearrangement occurs by OH and CO loss. Therefore, comparison between MS and TA helps in selection the proper pathway representing the fragmentation of this drug. This comparison successfully confirmed by MO calculation. Finally, the effect of fluorine atom on the stability of the drug was discussed.

Keywords Ciprofloxacin (CPF) · Mass spectra (MS) · Thermal analysis (TA) · MO calculation · Structure reactivity relationship

N. E. A. El-Gamel (✉)
Department of Chemistry, Faculty of Science, Cairo University, Giza 12613, Egypt
e-mail: nadinealy@hotmail.com

M. F. Hawash · M. A. Fahmey
Nuclear Physics Department, Nuclear Research Centre, AEA, Cairo 13759, Egypt

Introduction

Ciprofloxacin (CPF, $C_{17}H_{18}FN_3O_3$, MW = 331) (Fig. 1) is a synthetic chemotherapeutic antibiotic drug class [1]. It belongs to fluoroquinolones antibacterial. It attacks bacteria, such as anthrax, by interfering with the enzymes that cause DNA to rewind after being copied, which stops DNA and protein synthesis. In vitro potency against the target enzymes is highly enhanced due to the presence of fluorine substituent on quinolone [2]. This could be promising for further biological activity studies owing to their potential penetration into bacterial cell. CPF has become the gold standard of the first generation of fluoroquinolones, showing optimal antibacterial activity particularly against the gram negative organisms.

The mass spectrometry has become a powerful tool for drug metabolism studies [3] because it provides a large amount of structural information with little expenditure of sample. In electron impact (EI) mass spectrum, the fragmentation consists of series of competitive and consecutive unimolecular fragmentation [4]. The fragmentation of ionized molecule depends mainly on their internal energy

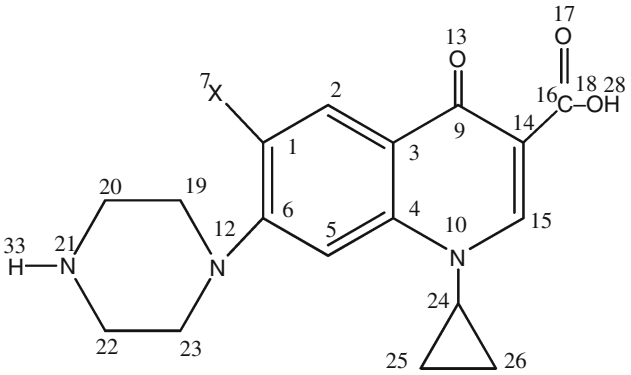

Fig. 1 Structural and numbering system of CPF

[5]. At 70 eV, the spectra are very complex; it is difficult to uncover all the competing and consecutive fragmentation reaction.

Thermogravimetric TG/DTG analysis used to provide quantitative information on weight losses due to decomposition and/or evaporation of low molecular materials as a function of time and temperature. By applying mass spectrometric analysis [6–8], the nature of the released volatilizes maybe deduced, which facilitate the interpretation of thermal degradation processes. In addition to that, computational quantum chemistry can provide additional information about the atoms and bonds, which can be used successfully to explain the experimental results [9]. Application of computational quantum chemistry in addition to experimental results (MS and TA) gives valuable information about the atoms and bonds which helps in the description and prediction of primary fragmentation site of cleavage and subsequent one [10–13].

The aim of this study is to focus on further application of our previously work [10–13] on CPF drug. This study includes a correlation between mass spectral fragmentation and thermal analysis (TA) degradation of the drug and comparing the experimental data with the theoretical Molecular Orbital (MO) calculation to identify the weakest bonds ruptured during both mass and thermal studies. In a summary, the choice of the correct pathway of such fragmentation is crucial to decide the active sites of drug which can be responsible for its chemical, biological, and medical reactivity.

Experimental

Elemental analysis (C, H, and N) were performed using a Foss Heraeus "CHN-O-RAPID" analyzer. IR spectra were obtained from dispersions in KBr using NICOLET 510 spectrometer. NMR spectra were recorded on a BRUKER DPX 400 instrument at room temperature (d_6-DMSO solution with TMS as internal standard. UV–Vis spectrophotometric measurements were carried out using automated spectrophotometer UV–Vis Thermo Fischer Scientific Model Evolution 60 ranged from 200 to 900 nm.

Measurements

Mass spectrometry (MS)

Electron ionization mass spectrum of CPF is obtained using Shimadzu GC-MS-Qp 1000 PX quadruple mass spectrometer with electron multiplier detector equipped with GC–MS data system. The direct probe (DP) for solid material was used in this study. The sample was put into a glass sample micro vial, by a needle (≈ 1 μg max), the vial installed on the tip of the DP containing heating cable and inserted into the evacuated ion source. The sample was ionized by electron beam emitted from the filament, the generated ions being effectively introduced into the analyzer by the focusing and extractor lenses system. The MS was continuously scanned and the obtained spectra were stored. Electron ionization mass spectra were obtained at ionizing energy value of 70 eV, ionization current of 60 μA, and vacuum is better than 10^{-6} torr.

Thermal analyses (TA)

The thermal analyses of CPF drug were made using conventional thermal analyzer (Shimadzu system of DTA-50 and 30 series TG-50). The heating rate, in an inert argon atmosphere, was 10 °C min^{-1} and employed a sample mass loss of 5 mg. The heat responds of the change of the sample were measured from room temperature up to 600 °C. These instruments were calibrated using indium metal as a thermal stable material. The reproducibility of the instrument reading was determined by repeating each experiment more than twice.

Computational method

The MO calculations were performed using semi-empirical MO calculation. The method used in these computations is the parametric method (PM-3) described by Stewart [14]. The default criteria for terminating all optimizations were increased by a factor of 100 (keyword PRECISE). Vibrational frequencies were computed for the studied structures (keyword FORCE) so as to check whether the newly designed geometries are local minima. All the MO calculations were carried out at the restricted Hartree–Fock level for the neutral molecule of gliclazide while the unrestricted Hartree–Fock level were carried out for its cation by using PM-3 method followed by full optimization of all geometrical variables (bond lengths, bond angles, and dihedral

angles), without any symmetry constraint. All structures were optimized to a gradient norm 0.01–0.05, using the eigenvector following (EF) routine [15]. All the semi-empirical MO calculations were performed with the MOPAC2000 software package [16] implemented on an Intel Pentium IV 3.0 GHz computer.

Results and discussion

The study of the chemistry and reactivity of CPF drug is of great interest due to its potential applications in medicine. The approach of the thermal decomposition mechanism has emerged as a valuable route for understanding the chemical process that shared in biological systems. It is difficult to establish the exact major fragmentation pathway in EI using conventional MS, therefore, with combining the above two techniques and the data obtained from the MO calculation, it is possible to understand the following topics:

1. Stability of the drug under thermal degradation in solid state and mass spectral fragmentation in gas phase.
2. Prediction of the primary site of fragmentation and subsequent bond cleavage.
3. The correct pathway in both techniques.
4. The process occurred in biodegradation of the drug or its derivatives in vivo system and metabolites.

IR spectra

The IR of CPF exhibit band in the range 1735–1707 cm^{-1} is ascribed to the vibration of carboxylic C=O group. The intense band at 1617 cm^{-1} could be assigned as $\nu(C=O)_p$ (p = pyridone). The band in the region 3400–3200 cm^{-1} is assigned to O–H stretching vibrations. Two characteristic bands at 1556 and 1494 cm^{-1} that could be assigned as ν(O–C–O) asymmetric and symmetric stretching vibrations; respectively, moreover, it is very difficult to assign other vibrations in the spectra of CPF due to the presence of other numerous bands could be present in these regions [17] such as the presence of C=C stretching vibration of the aromatic rings around 1620 cm^{-1} and the CH bending vibrations (νCH) in the region between 1440 and 1550 cm^{-1} and the stretching vibration of the quinolone ring system (ν ring) around 1400 cm^{-1}.

NMR analysis

The ^{1}H- and ^{13}C-NMR spectral assignments of CPF are given in Tables 1 and 2, respectively. The spectral data of the studied quinolones are very similar with very small shifts. The intramolecular hydrogen bond between the hydroxyl of the carboxyl group and the carbonyl of the pyridone nucleus also has an influence on the chemical shifts of C-4 and the CO signals, which are shifted downfield.

The implementation of the substituent on nitrogen changed the carbon chemical shift in the 2-position. For all carbons of the benzene ring, incremental chemical shifts elicited by the presence of the 3-substituted 4-quinolone ring, therefore similar data pertinent to the fused triazole or pyrazine ring, allow the prediction of chemical shifts in various fused multi-ring systems [18, 19].

UV–Vis

The absorption spectrum of CPF (0.25×10^{-5} mol/L) in ethanol is shown in Fig. 2. The spectra show a characteristic absorption band at 322 nm which could be due to

Table 2 ^{13}C-NMR chemical shifts of CPF in DMSO-d_6, shift δ in ppm

Position	Shift
C-2	148.0
C-3	106.9
C-4	176.2
C-4a	119.2
C-5	111.1
C-6	152.7
C-7	143.9
C-8	106.8
C-8a	139.0
COOH	165.6
N-1-R	36.0, 7.7
C-7-R	46.4, 42.6

Table 1 ^{1}H-NMR chemical shifts of CPF in DMSO-d_6, δ shift in ppm

Position	H-2	H-5	H-8	N-R	Piperazine
Shift	8.67 (s)	7.93 (d)	7.59 (d)	Cyclopropyl 3.85 (m) 1.15–1.37 (m)	3.34–3.69 (m)

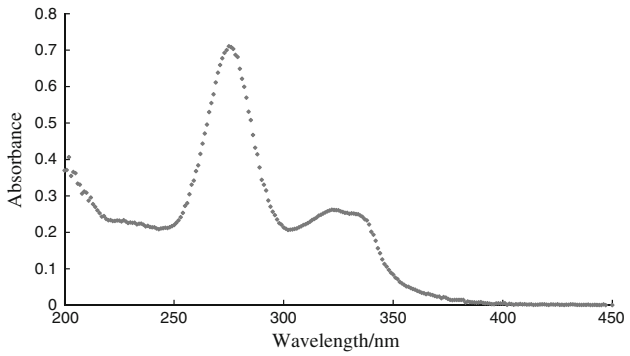

Fig. 2 The absorption spectra of CPF (0.25×10^{-5} mol/L) in ethanol

n–π^* (HOMO–LUMO) electronic transition [18]. The second maximum absorption is broad and observed at 275 nm, which can be attributed to the ring absorption. These transitions occur in related compounds such as unsaturated hydrocarbons which attached with oxygen atom as in carboxylic and ketone groups.

Thermal analysis

Only few references are reported on the thermal decomposition of the quinolones [20, 21]. The thermogravimetric analysis of the drug was recorded in the 40–700 °C range (Table 3, Scheme 1). The drug decomposes in three consecutive steps (Fig. 3). The first step is related to the loss of CO molecules (Found 9.73%, calcd. 8.45%).The DTA curve shows endothermic effect. The second mass loss occurs in the range 200–380 °C can be attributed to a loss of [$C_4H_8N_2H_2$ + CO] with an estimated mass loss of 34.44 (calcd. 34.44%); this step is accompanied with two endothermic peaks. The last decomposition within the temperature range 380–650 °C corresponds to the removal of the remaining drug as $C_{11}H_8FNO$ with a mass loss of 55.92 (calcd. 57.09%); this step is accompanied by the appearance of two successive endothermic peaks in the DTA curve (Table 3).

Mass spectral fragmentation

The 70 eV EI mass spectrum of CPF was recorded and investigated. A typical mass spectrum of CPF is shown in Fig. 4. The spectrum is complex and is characterized by some prominent fragment ions and many fragment ions between $m/z = 56$ and $m/z = 245$. The fragmentation pathways following electron impact was displayed in Scheme 2.

The mass spectrum of CPF using ESI-MS/MS techniques is illustrated in Fig. 5, this technique was used and mentioned by several authors to help in interpretation of formation of some fragment ions in the present mass spectrum [22].

The signal appears at $m/z = 331$ (R.I. = 55.8%) refers to appearance of the molecular ion $[C_{17}H_{19}FN_3O_3]^+$. The

Table 3 Thermoanalytical results for the investigated CPF

Stage	TG temperature range/°C	DTA peak temperature/°C	DTG temperature/°C	Found Mass loss%	(Calcd.) Mass loss	Assignment
1	40–200	146(+)	60, 140	9.73	(8.45)	Loss of CO
2	200–380	307(+), 355(+)	314	34.44	(34.44)	Loss of $C_4H_8N_2H_2$ + CO
3	380–650	449(+), 510(+)	571	55.92	(57.09)	Loss of $C_{11}H_8FNO$

(+) endothermic

Scheme 1 Thermal decomposition of CPF

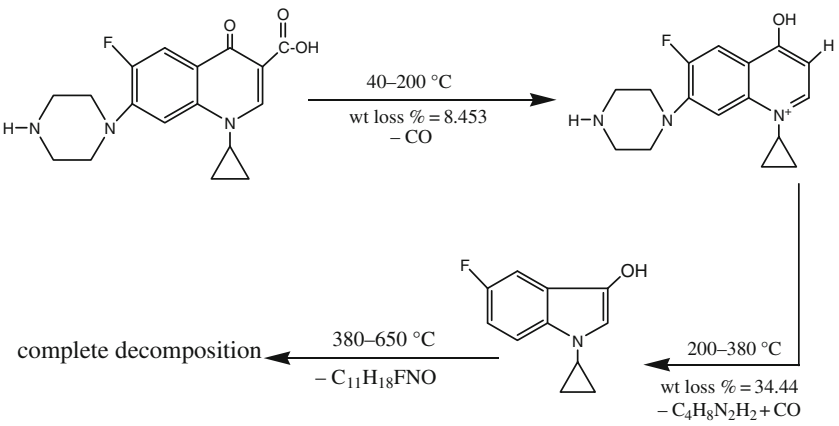

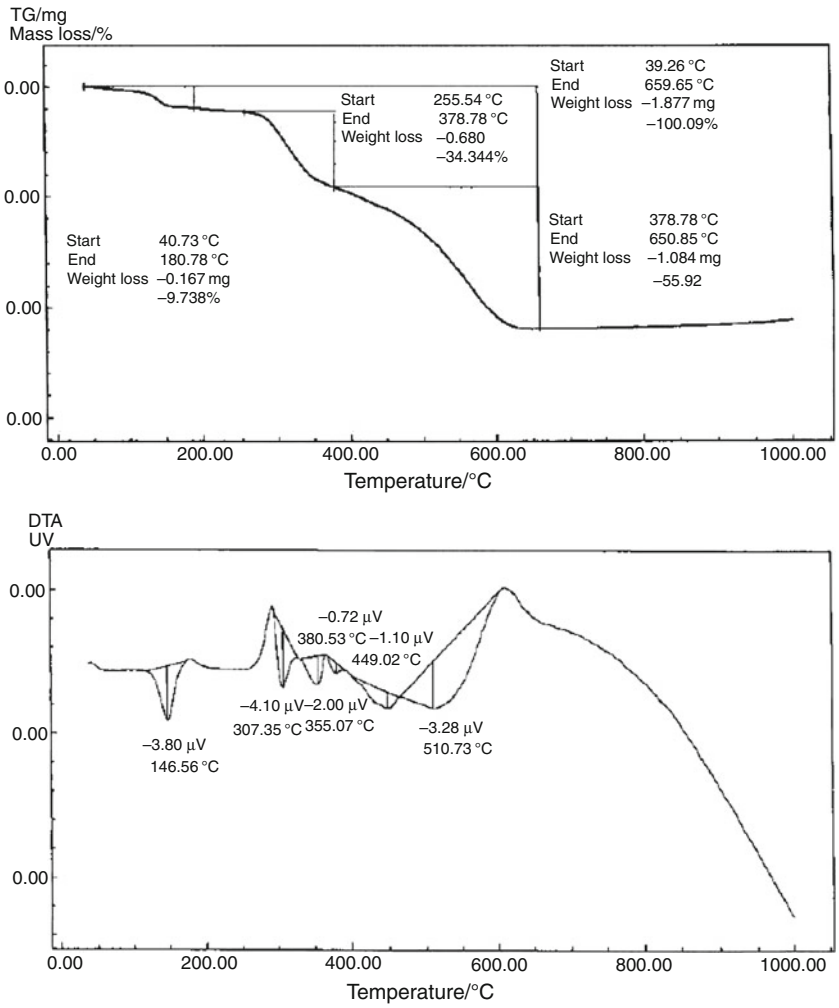

Fig. 3 Thermogravimetric analysis (TG/DTA) of CPF drug

relatively high intensity reflects the high stability of molecular ion of CPF. Two most prominent fragment ions observed in the mass spectrum of CPF at $m/z = 287$ (R.I. = 100%, base peak) and at $m/z = 245$ (R.I. = 97.7%) is apparently formed from molecular ion by loss of CO_2 and piperazine (C_2H_5N) ring forming $[C_{16}H_{18}FN_3O]^+$ and $[C_{14}H_3FN_2O]^+$ fragment ions (paths 1 and 2). The fragment ion ($m/z = 245$) can undergo further loss of piperazine, forming a common fragment ion $[C_{12}H_8FNO_2]^+$ ($m/z = 201$, R.I. = 15.0%) (path 3). Path 4 is due to loss of ethylene and water molecules forming $[C_{15}H_{13}FN_3O_2]^+$ fragment ion ($m/z = 286$, f. 288 R.I. = 72.1%). ESI-MS/MS and EI techniques represented similar results regarding the appearance of the main fragment ions as 332 $[M + H]^+$, 288, 245.

Computational MO calculation

Molecular orbital calculation gives valuable information about the structure and reactivity of the molecules, which actually be used to support the experimental evidence. Bond orders, bond length, charge distribution, bond strain, and heat of formation can be considered as the most potential parameters calculated from MO calculation. Herein, the calculations have been carried out on CPF neutral molecule (related to TA decomposition) and charged molecular ion (related to MS fragmentation) which is used for prediction of weakest bond rupture to follow the fragmentation pathways in both techniques (Table 4).

Figure 1 shows the numbering system of CPF skeleton that helps in ordering the bond length, bond order, bond strain, and charge distribution. Table 5 presents the values of bond length/Å, bond order, and bond strain/kcal mol^{-1}. From Table 5 we can conclude the following:

1. Small differences in bond length in CPF system upon ionization, indicating no appreciable change in the geometries upon ionization.
2. The lowest bond order (important for prediction of primary site of cleavage) observed at bond for both neutral (0.951) and positive species (0.923).
3. Upon ionization the stability of the molecule decreased by 190.42 kcal mol^{-1} ($\Delta H_f(-100.07)$–ΔH_f^+ (90.35)).

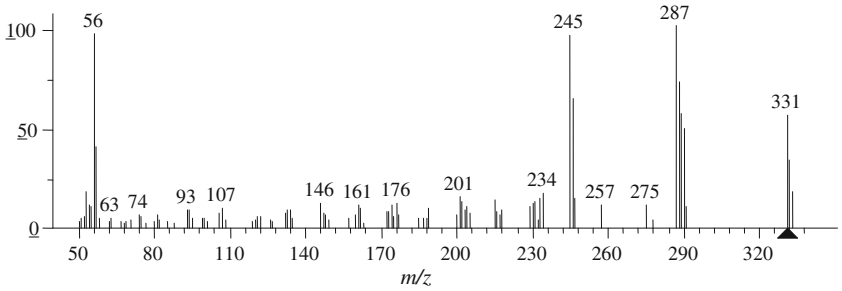

Fig. 4 Mass spectrum of CPF at 70 eV

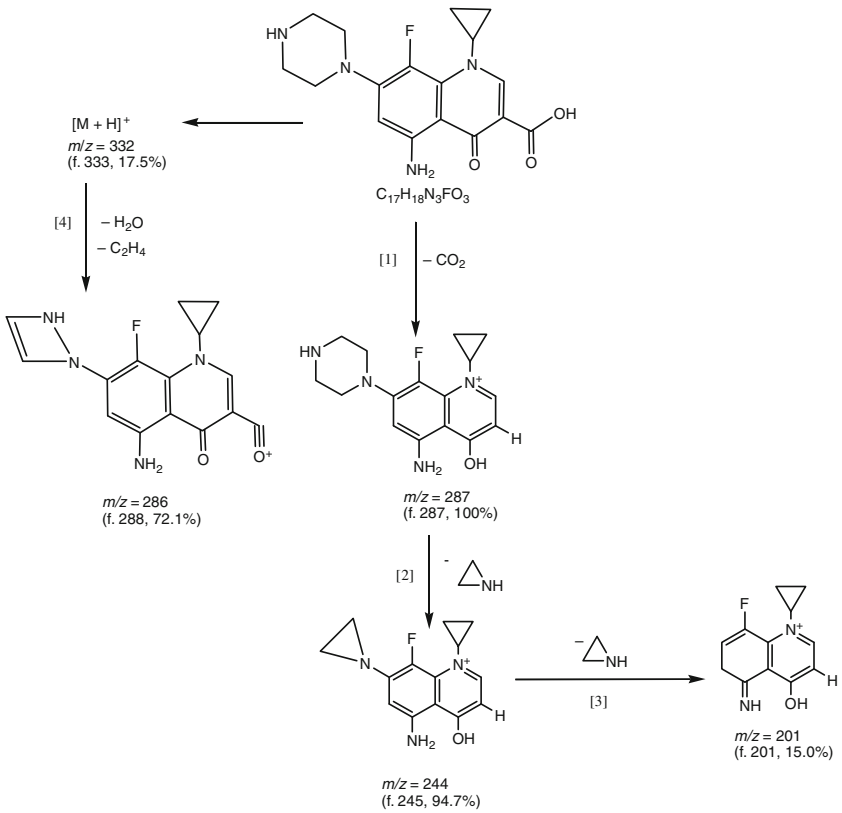

Scheme 2 Fragmentation pathway of principal fragmentation of CPF at 70 eV

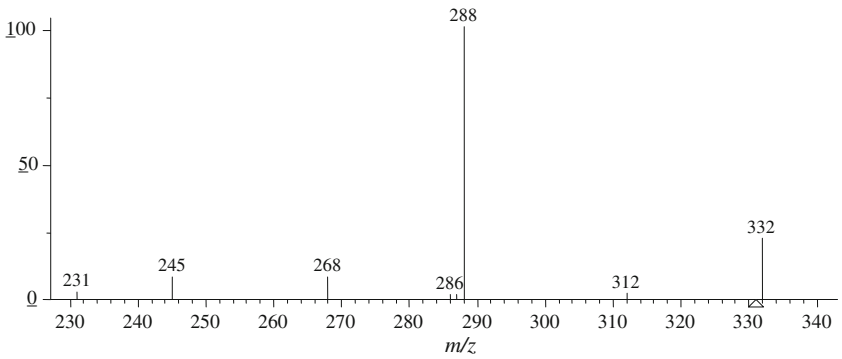

Fig. 5 CPF in the positive-ion ESI–MS/MS

The charge distributions on different atoms (C, N, O, and F) for neutral and charged species are summarized in Table 6. Significant change in the charge distribution with given system often takes place during the ionization process. For positive species, the highest positive charge are that located on C16 (0.461), C9 (0.399), and N10 (0.239) atoms, while for negative charges are that located on O13 (−0.227), O17 (−0.346), and O18 (−0.287). For neutral species, positive charges are that located on C16 (0.461), C9 (0.399), and N10 (0.239) while for negative charges at

Table 4 Comparison between some computed properties of CPF derivatives

Molecule	Dipole moment/debye	Electron affinity/eV	Heat of formation/kcal mol^{-1}	Ionization potential/eV
X=F (neutral)	6.99	0.775	−100.07	8.79
X=F (cation)	9.23	4.655	90.35	12.89
X=H (neutral)	6.89	0.542	−60.094	8.722
X=H (cation)	10.61	4.500	127.61	12.76
X=O (cation)	8.92	7.302	201.73	12.49

O17 (−0.413), O13 (−0.331), and C14 (−0.294). A highly difference in charge is observed on N12 (changed from 0.035 to 0.302) which could be a site of electron rupture due to ionization at values, 8.79 eV. No further changes in bond order was observed upon ionization except for C14–C16 the bond order decreases by 0.027.

Correlation between TA decomposition and MO calculation of neutral molecule

The thermal stability of the CPF with temperature change has not been studied before. As indicated, the determination of initial bond rupture would be an important step by using these calculations in predicative manner. On the base of MO calculating of values of bond order, bond length, and bond strain of the neutral system, one can expect that the C14–C16 bond has the lowest bond order at 0.951 in neutral system (bond length = 1.480 Å, bond strain = 0.009 kcal mol^{-1}).

In neutral and charged systems, the C14–C16 bond is the first site of bond rupture. Depending on MO calculation (Table 5), one can reveal that the C14–C16 bond is the first site of bond cleavage as a result of the lowest value of bond order at 0.951 (bond length = 1.480 Å and bond strain at 0.009 kcal mol^{-1}). Experimental TA data on CPF reveal that the first weight loss equals to 9.73% (wt loss) with calculated at 8.45%. This value of weight loss corresponding CO losses with OH-rearrangement at the temperature range 40–200 °C and peak at DTA at 146 °C. This wide range of decomposition may be due to slow fragmentation with small half life time, where the decomposition of molecules are continuously energized and deactivated by a gas evolution and the distribution of energy can be described by temperature [4], therefore the C14–C16 bond rupture with OH-rearrangement may need a continuous temperature. The rupture of CO with OH-rearrangement can be interpreted on the bases of electrostatic repulsion. The repulsion between O18 (−0.283) and H28 (0.223), distance 0.952 Å is less than between C18 (0.437) and O18 (−0.289) with distance 1.351 Å (i.e., 0.0696 < 0.0715).

Correlation between MS fragmentation and MO calculations of charged molecule

The scope of this investigation mainly proposed to predict the first and subsequent bond ruptures during the course of fragmentation of CPF drug using MS technique. The subsequent fragmentation in MS is determined to large extent by the initial bond rupture of molecular ion [10–13]. Many mass spectrometric techniques have been utilized helping in rationalized the correct pathways of the molecules, among these techniques, threshold measurement [23] and metastable abundance ratios have been used [24]. On the other hand, the interpretation of these computational results can be helpful to understand the mass fragmentation pathways especially in the gaseous phase due to the ease of handling by applying quantum mechanics chemistry [14–16]. Mass spectrum of CPF reveals (Scheme 1) three competitive and consecutive fragmentation pathways.

PM3 procedure reveals that the C14–C16 (Table 5) bond is the first site of bond cleavage (lowest bond order = 0.923, large bond length = 1.491 Å, bond strain = 0.009 kcal mol^{-1}. This bond cleavage accompanied by CO_2 loss, with H-rearrangement forming a fragment ion $[C_{16}H_{18}FN_3O]^+$ with $m/z = 287$ and R.I. = 100% (base peak). The high stability of this fragment ion arises from the presence of fluorine and nitrogen and oxygen lone pair atoms. Also, the formation and relative intensity of this fragment ion can be illustrated using ESI-MS/MS technique at $m/z = 288$ (protonated fragment ion). A high proliferation with R.I. = 100% is observed using both ESI-MS/MS and EI techniques, indicating very high stability in 70 EI and soft ionization techniques [22]. The rupture of CO_2 with H-rearrangement can be interpreted on the bases of electrostatic repulsion. The electrostatic repulsion between O18 (−0.289) and H28 (0.242) with distance = 0.953 Å is greater than C16 (0.437) and O18 (−0.289) with distance = 1.351 Å (i.e., 0.077 > 0.069). In summary, the molecule in charged system preferred to loss of CO_2 (H-rearr.) that the loss CO (OH-rearr.).

Table 5 Comparison of computed bond length/Å, bond order, and bond strain/kcal mol^{-1} using PM3 method for neutral and molecular cation

Bond	Bond length/Å		Bond order		Bond strain/kcal mol^{-1}	
	Neutral	Cation	Neutral	Cation	Neutral	Cation
C1–C2	1.391	1.395	1.453	1.422	0.005	0.005
C2–C3	1.399	1.388	1.355	1.424	0.006	0.005
C3–C4	1.406	1.438	1.346	1.184	0.024	0.024
C4–C5	1.404	1.390	1.341	1.409	0.091	0.095
C5–C6	1.396	1.423	1.412	1.282	0.159	0.158
C6–C1	1.421	1.455	1.281	1.141	0.205	0.203
C1–F7	1.347	1.334	0.993	1.034	0.002	0.002
C2–H8	1.100	1.105	0.952	0.947	0.001	0.001
C3–C9	1.485	1.499	0.962	0.941	0.040	0.042
C4–N10	1.430	1.405	1.068	1.182	0.174	0.162
C5–H11	1.107	1.106	0.937	0.939	0.021	0.020
C6–N12	1.440	1.370	1.064	1.331	0.423	0.428
C9–O13	1.221	1.214	1.852	1.910	0.002	0.002
C9–C14	1.473	1.472	0.977	0.974	0.000	0.000
C14–C15	1.358	1.347	1.673	1.761	0.003	0.001
C15–N10	1.396	1.420	1.180	1.111	0.049	0.049
C14–C16	1.480	1.491	0.951	0.923	0.009	0.011
C16–O17	1.220	1.214	1.781	1.846	0.009	0.009
C16–O18	1.351	1.351	1.066	1.068	0.014	0.015
N12–C19	1.491	1.486	0.968	0.972	0.141	0.149
C19–C20	1.529	1.536	0.971	0.953	0.099	0.098
C20–N21	1.482	1.475	0.996	1.010	0.022	0.020
N21–C22	1.481	1.475	0.998	1.011	0.029	0.024
C22–C23	1.532	1.538	0.968	0.952	0.025	0.024
C23–N12	1.490	1.488	0.976	0.974	0.177	0.175
N10–C24	1.471	1.476	0.970	0.963	0.219	0.203
C24–C25	1.510	1.511	0.968	0.971	1.133	1.122
C25–C26	1.498	1.494	0.994	1.002	2.949	2.942
C26–C24	1.506	1.510	0.979	0.978	1.149	1.139
C15–H27	1.107	1.102	0.942	0.950	0.000	0.000
O18–H28	0.952	0.953	0.919	0.916	0.000	0.001
C19–H29	1.109	1.113	0.972	0.965	0.001	0.002
C19–H30	1.117	1.119	0.953	0.952	0.006	0.004
C20–H31	1.107	1.109	0.976	0.974	0.001	0.002
C20–H32	1.109	1.110	0.973	0.974	0.003	0.003
N21–H33	0.999	0.998	0.975	0.975	0.001	0.001
C22–H34	1.107	1.109	0.976	0.975	0.001	0.001
C22–H35	1.109	1.110	0.973	0.974	0.002	0.002
C23–H36	1.109	1.113	0.972	0.965	0.003	0.002
C23–H37	1.111	1.113	0.968	0.966	0.005	0.005
C24–H38	1.112	1.110	0.950	0.956	0.002	0.002
C25–H39	1.097	1.097	0.971	0.975	0.002	0.001
C25–H40	1.096	1.097	0.975	0.977	0.001	0.000
C26–H41	1.102	1.098	0.962	0.973	0.001	0.001
C26–H42	1.095	1.097	0.974	0.976	0.000	0.000

Table 6 Computed hybridization and atomic charge distribution of CPF derivatives

Atom	Hybridization	Partial charge			
		X=F (neutral)	X=F (cation)	X=H (neutral)	X=H (cation)
C1	*sp*2	−0.005	0.130	−0.187	−0.064
C2	*sp*2	−0.020	−0.068	0.015	−0.033
C3	*sp*2	−0.191	−0.048	−0.212	−0.041
C4	*sp*2	−0.014	−0.003	−0.006	−0.010
C5	*sp*2	−0.213	−0.268	−0.222	−0.236
C6	*sp*2	0.004	−0.030	0.022	−0.027
X7=F	*sp*2	−0.084	−0.044	0.122	0.138
H8	*s*	0.143	0.173	0.124	0.156
C9	*sp*2	0.399	0.351	0.402	0.354
N10	*sp*2	0.239	0.292	0.220	0.255
H11	*s*	0.134	0.156	0.133	0.153
N12	*sp*2	0.035	0.302	0.022	0.319
O13	*sp*2	−0.331	−0.228	−0.336	−0.231
C14	*sp*2	−0.294	−0.210	−0.298	−0.233
C15	*sp*2	−0.050	−0.066	−0.035	−0.047
C16	*sp*2	0.461	0.437	0.462	0.441
O17	*sp*2	−0.413	−0.346	−0.414	−0.360
O18	*sp*2	−0.283	−0.287	−0.285	−0.286
C19	*sp*3	−0.149	−0.192	−0.119	−0.166
C20	*sp*3	−0.113	−0.104	−0.118	−0.107
N21	*sp*3	−0.052	−0.008	−0.052	−0.007
C22	*sp*3	−0.118	−0.108	−0.118	−0.107
C23	*sp*3	−0.121	−0.160	−0.118	−0.164
C24	*sp*3	−0.158	−0.200	−0.161	−0.196
C25	*sp*3	−0.156	−0.133	−0.141	−0.134
C26	*sp*3	−0.141	−0.109	−0.134	−0.110
H27	*s*	0.140	0.156	0.134	0.158
H28	*s*	0.223	0.242	0.222	0.241
H29	*s*	0.069	0.099	0.066	0.098
H30	*s*	0.109	0.127	0.081	0.103
H31	*s*	0.070	0.098	0.068	0.098
H32	*s*	0.069	0.084	0.070	0.085
H33	*s*	0.049	0.066	0.048	0.067
H34	*s*	0.066	0.094	0.066	0.096
H35	*s*	0.066	0.083	0.068	0.084
H36	*s*	0.070	0.096	0.067	0.097
H37	*s*	0.071	0.097	0.074	0.101
H38	*s*	0.121	0.127	0.109	0.122
H39	*s*	0.093	0.097	0.097	0.097
H40	*s*	0.089	0.095	0.084	0.092
H41	*s*	0.094	0.101	0.096	0.103
H42	*s*	0.092	0.106	0.087	0.103

Conclusions

The correlation study of TA and MS of CPF showed a great facility to understand the possible starting decomposition behavior of the drug in both techniques. This comparison exhibits the agreement and disagreement on the fragmentation pathways. Consequently, the effect of such fragmentation on the drug behavior in human body

can be expected and also its metabolites can easily be identified.

From studying the TA and MS techniques of CPF, the C14–C16 bond is found to be the first site of rupture, where the first weight loss = 8.45% at temperature range 40–200 °C is observed, with an endothermic effect at 146 °C. This weight loss corresponds to loss of CO with OH-rearrangement at around 160 °C (Scheme 1).

References

1. Nelson JM, Chiller TM, Powers JH, Angulo FJ. Fluoroquinolone-resistant Campylobacter species and the withdrawal of fluoroquinolones from use in poultry: a public health success story. Clin Infect Dis. 2007;4:977–80.
2. Alovero FL, Pan X-S, Morris JE, Manzo RH, Fisher LM. Engineering the specificity of antibacterial fluoroquinolones: benzenesulfonamide modifications at C-7 of ciprofloxacin change its primary target in *Streptococcus pneumoniae* from topoisomerase IV to gyrase. Antimicrob Agents Chemother. 2000;44(2):320–5.
3. Larsen BS, McEwen C, editors. Mass spectrometry of biological materials. 2nd ed. Revised and Expanded. New York: Marcel Dekker; 1998.
4. Levsen K. Progress in mass spectrometry, Vol. 4. Fundamental aspects of organic mass spectrometry. Weiheim, New York: Verlag Chemie; 1978.
5. Bourcier S, Hoppiliard Y. Fragmentation mechanisms of protonated benzylamines. Electrospray ionisation-tandem mass spectrometry study and ab initio molecular orbital calculations. Eur J Mass Spectrom. 2003;9:351–60.
6. Fahmey MA, Zayed MA, Keshek YH. Comparative study on the fragmentation of some simple phenolic compounds using mass spectrometry and thermal analyses. Thermochem Acta. 2001;366:183–8.
7. Fahmey MA, Zayed MA. Phenolic-iodine redox products: mass spectrometry, thermal and other physico-chemical methods of analyses. J Therm Anal Calorim. 2002;67:163–75.
8. Fahmey MA, Zayed MA, El-Shobaky HG. Study of some phenolic-iodine redox polymeric products by thermal analyses and mass spectrometry. J Therm Anal Calorim. 2005;82:137–42.
9. Somogyi A, Gomory A, Vekey K, Tamas J. Use of bond orders and valences for the description and prediction of primary fragmentation processes. Org Mass Spectrom. 1991;26:936–8.
10. Zayed MA, Fahmey MA, Hawash MF. Investigation of malonanilide and its dinitro-isomers using thermal analyses, mass spectrometry and semi-empirical MO calculation. Egypt J Chem. 2005;48:43–57.
11. Zayed MA, Fahmey MA, Hawash MF. Investigation of diazepam drug using thermal analyses, mass spectrometry and semi-empirical MO calculation. Spectrochim Acta A. 2005;61:799–805.
12. Zayed MA, Hawash MF, Fahmey MA. Structure investigation of codeine drug using mass spectrometry, thermal analyses and semi-emperical molecular orbital (MO) calculations. Spectrochim Acta A. 2006;64:363–71.
13. Zayed MA, Fahmey MA, Hawash MF, El-Habeeb AA. Mass spectrometric investigation of buspirone drug in comparison with thermal analyses and MO-calculations. Spectrochim Acta A. 2007;67:522–30.
14. Stewart JJP. Optimization of parameters for semi-empirical methods I. Method. J Comput Chem. 1989;10:209–20.
15. Baker J. An algorithm for the location of transition states. J Comput Chem. 1986;7:385–95.
16. Stewart JJP. Software package MOPAC 2000, Tokyo: Fujitsu Limited; 1999.
17. Milata V, Ilavsky D, Goljer I, Zalibera L. Thermal cyclocondensation of ethyl (1-methyl-5- and 6-benzimidazolyl/benzotriazolyl)aminomethylenepropanedioates. Collect Czech Chem Commun. 1994;59:1145–52.
18. Song C-H, Ryu H-W, Park J-K, Ko T-S. Mechanism of DNA gyrase inhibition by quinolones: I. Spectral analysis for nalidixic acid polymorphism. Bull Korean Chem Soc. 1999;20:727–30.
19. Milata V, Ilavsky D, Chudik M, Zalibera L, Lesko J, Seman M, Belicova A. Gould-Jacobs reaction of 6-amino-2, 3-diphenylquinoxaline. Mon Chem. 1995;126:1349–58.
20. Mazuel C. Norfloxacin. In: Florey K , editor. Analytical profiles of drugs substances. Vol. 20. San Diego: Academic press; 1991. p. 557–600.
21. Šuštar B, Bukovec N, Bukovec P. Polymorphism and stability of norfloxacin, (1-ethyl-6-fluoro-1, 4-dihydro-4-oxo-7-(1-piperazinil)-3-quinolinocarboxylic acid. J Therm Anal. 1993;40:475–81.
22. Zayed MA, Nour El-Dien FA, Hawash MF, Fahmey MA. Mass spectra of gliclazide drug at various ion sources temperature. Its thermal behavior and molecular orbital calculations. J Therm Anal. 2010;102:305–12.
23. Johnson PM, Zhu L. Mass analyzed threshold ionization: structural information for a mass spectrum and mass information for ionic spectroscopy. Int J Mass Spectrom Ion Process. 1994;131:193–209.
24. Cooks RG, Beynon JH, Caprioli RM, Laster GR. Metastable ions. Amsterdam: Elsevier; 1973. p. ix–296.